Novel Insertion Mutation in KCNJ5 Channel Produces Constitutive Aldosterone Release From H295R Cells

Iris Hardege, Shengxin Xu, Richard D. Gordon, Andrew J. Thompson, Nichola Figg, Michael Stowasser, Ruth Murrell-Lagnado, and Kevin M. O'Shaughnessy

Divisions of Experimental Medicine and Immunotherapeutics (I.H., K.M.O.) and Cardiovascular Medicine (N.F.), Department of Medicine, and Department of Pharmacology (A.J.T., R.M.-L.), University of Cambridge, Cambridge CB2 2QQ, United Kingdom; and Endocrine Hypertension Research Centre (S.X., R.D.G., M.S.), University of Queensland School of Medicine, Greenslopes and Princess Alexandra Hospitals, Brisbane 4072, Australia

Primary aldosteronism accounts for 5%–10% of hypertension and in a third of cases is caused by autonomous aldosterone production by adenomas (APA). Somatic mutations in the potassium channel encoded by *KCNJ5* have been detected in surgically removed APAs. To better understand the role of these mutations, we resequenced the *KCNJ5* channel in a large Australian primary aldosteronism cohort. *KCNJ5* mutations were detected in 37 APAs (45% of the cohort), including previously reported E145Q (n = 3), G151R (n = 20), and L168R (n = 13) mutations. In addition, we found a novel 12-bp in-frame insertion mutation (c.414–425dupGCTTTCCTGTTC, A139_F142dup) that duplicates the AFLF sequence in the pore helix upstream of the selectivity filter. Expressed in Xenopus oocytes, the A139_F142dup mutation depolarized the oocytes and produced a G-protein-sensitive Na^+ current with altered K^+ selectivity and loss of inward rectification but retained Ba^{2+} sensitivity. Transfected into H295R cells, A139_F142dup increased basal aldosterone release 2.3-fold over the wild type. This was not increased further by incubation with angiotensin II. Although the A139_F142dup mutant trafficked to the plasma membrane of H295R cells, it showed reduced tetramer stability and surface expression compared with the wild-type channel. This study confirms the frequency of somatic *KCNJ5* mutations in APAs and the novel mutation identified (A139_F142dup) extend the phenotypic range of the known *KCNJ5* APA mutations. Being located in the pore helix, it is upstream of the previously reported mutations and shares some features in common with selectivity filter mutants but additionally demonstrates insensitivity to angiotensin II and decreased channel stability. **(*Molecular Endocrinology* 29: 1522–1530, 2015)**

Up to 10% of hypertension cases are now attributed to primary aldosteronism (PA), which is driven by autonomous aldosterone production from the adrenals. This has led to the current screening guidelines for PA that emphasize adrenal vein sampling to identify unilateral aldosterone production (1). Recent series report that approximately a third of the PA cases are caused by unilateral aldosterone-producing adenomas (APAs), with most of the remainder due to bilateral adrenal hyperplasia (2).

With the exception of the rare, glucocorticoid-remediable familial variety of PA, the molecular processes driving PA and APAs were unclear until the recent application of whole-exome sequencing. Its application to APAs in 2011 first identified somatic mutations in the G protein-regulated K channel (GIRK4; also called Kir 3.4) encoded by the *KCNJ5* gene (3). Since then, somatic mutations in *KCNJ5* have been reported in surgically recovered APAs from a number of cohorts of PA patients. In Caucasian populations their frequency is typically approximately 30%–40% (4), but the prevalence appears to be much higher in Japanese (65%) and Chinese (>70%) cohorts (5–7). The reasons for these demographic differences are

ISSN Print 0888-8809 ISSN Online 1944-9917
Printed in USA

Received July 17, 2015. Accepted September 1, 2015.
First Published Online September 4, 2015

Abbreviations: APA, aldosterone-producing adenoma; APCC, adrenal cortical cell; CCh, carbachol; E_{rev}, reversal potential; GFP, green fluorescent protein; GIRK4, G protein-regulated K channel; HEK, human embryonic kidney; I-V, current-voltage steps; M2R, muscarinic receptor 2; NES, NaCl, KCl, $CaCl_2$, $MgCl_2$, glucose, and HEPES; PA, primary aldosteronism; PEI, polyethylenimine; TBS, Tris-buffered saline.

unclear. Germline mutations have also been identified in *KCNJ5* as the cause of rare syndromic forms of familial PA (familial hyperaldosteronism type III), thus emphasizing further the role of this channel in aldosterone-dependent hypertension (4, 8, 9).

The function of the GIRK4 channel is best understood in the atria in which it is involved in mediating the cholinergic effects of the vagus nerve on the heart (10). Here it forms a K-selective channel by heterotetramerizing with GIRK1 (11). Prior to 2011, it was not appreciated that GIRK4 is expressed in the adrenal cortex and only subsequently confirmed on the surface membrane of zona glomerulosa cells (3, 12). The somatic *KCNJ5* mutations reported to date have been either within or close to the selectivity filter of the channel and cause a loss of K^+ selectivity that results in Na^+ influx and depolarization of the cell (3, 4, 13). It is still debatable whether these mutations affect cell growth and, if so, whether this involves calcium loading the adrenal cortical cells (4).

To explore the role further of *KCNJ5* mutations in APAs, we have systematically sequenced the exome of *KCNJ5* in our collection of surgically excised APAs. Our goal was to confirm the frequency of known *KCNJ5* mutations in our cohort but also identify new mutations that may have novel phenotypes to extend our understanding of their pathogenic role in aldosterone release from APAs.

Materials and Methods

KCNJ5 Resequencing

The APAs consisted of consecutive surgical adrenal specimens recovered at Princess Alexandra Hospital or Greenslopes Private Hospital (Brisbane, Australia). Both are specialist endocrine hypertension referral centers and receive patients primarily from Queensland, but also from other states of Australia. Tissue collection from this cohort of referrals has been ongoing for more than a decade and an EDTA sample of peripheral blood is routinely collected from each patient. The genetic study was approved by the Ethics Committee of University of Queensland, and informed consent for DNA collection and the genetic study was obtained from all participants. Genomic DNA was extracted by standard methods. The genomic DNA from the APAs was recovered for somatic mutation detection as well as genomic DNA from peripheral venous blood or adjacent non-adenoma adrenal tissue to confirm that any mutations detected in the APA were not present in the germline. The entire coding sequence (exons 2–3) and flanking regions of *KCNJ5* were amplified by PCR (see the online-only Supplemental Materials and Methods for the PCR primer sequences) and the products purified with a one-column clean-up method (www.promega.co.uk). PCR was performed on 25 ng DNA in a final volume of 30 μL containing: 1.5 mM $MgCl_2$, 0.2 mM of each primer, 0.2 mM deoxynucleotide triphosphate, and 1.0 U of Taq DNA polymerase (www.lifetechnologies.com). Sanger sequencing of the purified products was undertaken on either the Applied Biosystems 3730xl DNA analyzer or Beckman CEQ8000 platforms.

Cloning

Wild-type green fluorescent protein (GFP)-tagged *KCNJ5* was sourced in the pCMV-AC-GFP expression vector from Origene (www.origene.com) and untagged human *KCNJ5* in pGEMHE was obtained from M. Murthy (University of Cambridge). PCR-based, site-directed mutagenesis was carried out using Phusion polymerase to generate the 12bp duplication (A139_F142), plasmids were sequenced to confirm insertion (www.sourcebioscience.com).

Expression in Xenopus oocytes

RNA was synthesized using T7 mMachine kit (www.lifetechnologies.com) from pGEM-KCNJ5 vectors linearized by *Pst*I digestion. RNA was cleaned using the RNeasy clean-up kit (www.qiagen.com) and 50 ng of RNA per construct was injected per defolliculated oocyte (www.ecocyte-us.com) in 50 nL. Postinjection oocytes were incubated in ND96 (96 mM NaCl, 1 mM $MgCl_2$, 3 mM KCl, 5 mM HEPES) at 16°C.

Two-electrode voltage clamp

Two days after the injection, *Xenopus* oocytes were clamped at −80 mV, as detailed previously (13, 14), using borosilicate microelectrodes (GC120TF-10; www.harvardapparatus.co.uk) generated by a two-stage horizontal puller (model P-87, www.sutter.com) to achieve 1–2 MΩ resistance and then filled with 3 M KCl. Oocytes were perfused with ND96 at a constant rate of 6 mL/min with solution exchange by a gravity-fed system with the same flow rate. Current-voltage steps (I-V) were obtained in each solution once a steady-state current was achieved. Oocytes were exposed to the following solutions: 98 mM K^+ (96 mM KCl, 11 mM D-glucose, 1 mM $MgCl_2$, and 5 mM HEPES); 50/50 (49 mM KCl, 49 mM NaCl, 5.5 mM D-glucose, 1 mM $MgCl_2$, and 5 mM HEPES); N-methyl-D-glucamine (96 mM **N-methyl-D-glucamin, 1 mM $MgCl_2$**, 5 mM HEPES, and 25 mM D-glucose).

Data analysis and curve fitting was performed with Prism 6 (www.graphpad.com/scientific-software/prism). To compare I-V plots, the current for each oocyte was normalized to the maximal current and expressed as mean I/Imax ± SEM for a series of oocytes.

Expression in H295R cells

H295R cells were maintained as described previously (14, 15). *KCNJ5* constructs in the pCMV-AC-GFP vector were transiently expressed by electroporation using the mirus nucleofection solution (www.mirusbio.com) and a Lonza transfection machine setting T-020 (www.lonza.com). Electroporated cells were plated in 96-well plates for 24 hours before exchanging into culture medium with or without 10 nM angiotensin II (www.sigmaaldrich.com). After 24 hours, supernatant was collected for aldosterone assays (www.cisbio.com/drug-discovery/aldosterone-assay) and cell viability measured using an dimethylthiazoldiphenyltetra-zoliumbromide viability assay; cells were treated with 12 mM 3-(4,5-dimethylthiazol-2-yl)-2,5-diphenyltetrazolium bromide in phenol-free medium for 3 hours, supernatant discarded, and precipitate resuspended in dimethylsulfoxide prior to absorbance measurement at 540 nm.

Expression in human embryonic kidney (HEK)-293T and HeLa cells

Cells were maintained in DMEM supplemented with 2 mM glutamine, 100 U/mL penicillin, 100 μg/mL streptomycin, and 10% fetal bovine serum (www.sigmaaldrich.com). The *KCNJ5*-GFP constructs mentioned previously were transiently expressed by polyethylenimine (PEI) transfection (www.polysciences.com); PEI (high potency linear PEI, molecular weight 40 000) at 1 mg/mL in 20 mM HEPES (pH 7.5) was mixed with 2 μg of DNA and OptiMEM medium (at a 3:1:100 ratio) for 15 minutes and then added dropwise to a monolayer of 70% confluent cells.

Confocal microscopy

HeLa cells were grown overnight on 0.01% poly-L-lysine (www.sigmaaldrich.com) coated 12 mm glass coverslips before transfection with PEI, as described above. Forty-eight hours after the transfection, cells were washed once in PBS prior to fixation in 4% formaldehyde-PBS for 10 minutes at room temperature. Cells were then washed twice in NES (140 mM NaCl; 5 mM KCl; 2 mM $CaCl_2$; 1 mM $MgCl_2$; 10 mM glucose; 10 mM HEPES, pH 7.4), incubated for 10 minutes with WGA-594CW (www.biotium.com), washed twice in NES and mounted with 4′,6′-diamino-2-phenylindole Vectashield mounting medium (www.vectorlabs.com).

Biotinylation

HEK293T cells in six-well plates were washed once in NES and placed on ice. Cells were incubated in 0.2 mg/mL NHS-biotin (www.thermofisher.com) for 45 minutes on ice before quenching with Tris buffer (25 mM Tris-HCl; 150 mM NaCl; 10 mM EDTA, pH 7.4). Cells were removed from the plate and centrifuged at 200 g for 5 minutes at 4°C. Supernatant was discarded and cells incubated in solubilization buffer (25 mM Tris-HCl; 150 mM NaCl; 10 mM EDTA; 1% Triton X-100, pH7.4) with protease inhibitors (www.roche.co.uk) at 4°C with agitation for 1 hour. The resulting lysate was cleared by centrifugation at 14 k rpm 4°C for 1 hour. Thirty microliters of streptavidin beads (www.thermofisher.com) per sample were washed once in wash buffer (25 mM Tris-HCl; 150 mM NaCl; 10 mM EDTA; 1% Triton X-100, pH 7.4), centrifuged at 1400 rpm for 5 minutes at 4°C and supernatant removed. Fifty microliters cell lysate was stored at −20°C (total protein fraction), and the remaining supernatant was added to streptavidin beads and incubated with agitation for 2 hours at 4°C. Beads were then pelleted at 14 000 rpm for 5 minutes at 4°C and washed three times in wash buffer before resuspending the pellet in sample buffer (www.lifetechnologies.com).

Western blotting

Ten micrograms of protein lysates were separated by SDS-PAGE. Prior to loading, samples were heated at 70°C for 10 minutes in 1× SDS sample buffer and 1× reducing agent buffer (www.lifetechnologies.com) to a total volume of 20 μL/well. Samples and 5 μL of Precision Plus molecular weight ladder (www.bio-rad.com) were then loaded onto a Bolt 4%–12% Bis-Tris Plus gel (www.lifetechnologies.com) and run at 165 V in 1× MES running buffer (www.lifetechnologies.com) for 35 minutes or until the dye front reached the end of the gel. Resolved proteins were then transferred to 0.22 μM nitrocellulose membrane using the iblot2 (www.lifetechnologies.com) at 20 V for 7 minutes. Membranes were incubated in 5% milk in Tris-buffered saline (TBS) for 1 hour at room temperature. Anti-GIRK4 (HPA017353 at 1:1000 dilution; www.sigmaaldrich.com) and antiactin (MA5-15739 at 1:1000 dilution; www.pierce-antibodies.com) were incubated overnight at 4°C in 5% milk in TBS-Tween (0.1% Tween 20) and then washed six times in TBS-Tween 20. Secondary antibodies, donkey antirabbit 800CW (926-32213 at 1:5000 dilution; www.licor.com) and goat antimouse Alexa680 (A-21058 at 1:5000 dilution; www.lifetechnologies.com) were incubated in TBS-Tween 20 for 1 hour at room temperature in the dark and then washed six times in TBS-Tween 20. Membranes were imaged using the LiCor Odessey system (www.licor.com).

Immunohistochemistry

Formaldehyde-fixed, paraffin-embedded cortex and tumor sections were stained with anti-GIRK4 (HPA017353; www.sigmaaldrich.com), as described in the online-only Supplemental Materials and Methods.

Statistical analysis

All data are shown as mean ± SEM unless indicated otherwise. Significance was set at $P < .05$ and calculated using the stats package in Prism 6 (http://www.graphpad.com/scientific-software/prism/).

Results

Mutation screening of *KCNJ5*

Sequencing the entire coding region of *KCNJ5* from the 82 surgically removed APAs identified the two most commonly reported selectivity filter mutants, G151R (n = 20) and L168R (n = 13), as well as the rarer E145Q (n = 3). In addition, we identified a single APA containing a novel in-frame insertion mutant that caused a 12-bp duplication of the AFLF motif encoded by residues A139-F142 in human *KCNJ5* (Figure 1). The adrenal cortex adjacent to the APA had a wild-type *KCNJ5* sequence, confirming that the mutation was somatic (Figure 1).

Patient characteristics

The clinical characteristics of patients in the APA cohort are shown in Supplemental Table 1. They were all of Caucasian ethnicity. The subject with the APA containing the novel 12-bp duplication was a 54-year-old male who had severe PA with resistant hypertension, hypokalemia, and elevated aldosterone to renin ratio (aldosterone, 490 pmol/L; renin, 2 mU/L; aldosterone to renin ratio 296). The aldosterone was not suppressible on fludrocortisone suppression testing, and it fell on standing as we have observed previously in patients with APAs carrying *KCNJ5* mutations (16). On computed tomography scanning of his adrenal gland, he had an 11-mm adenoma in his left adrenal gland, and aldosterone production later-

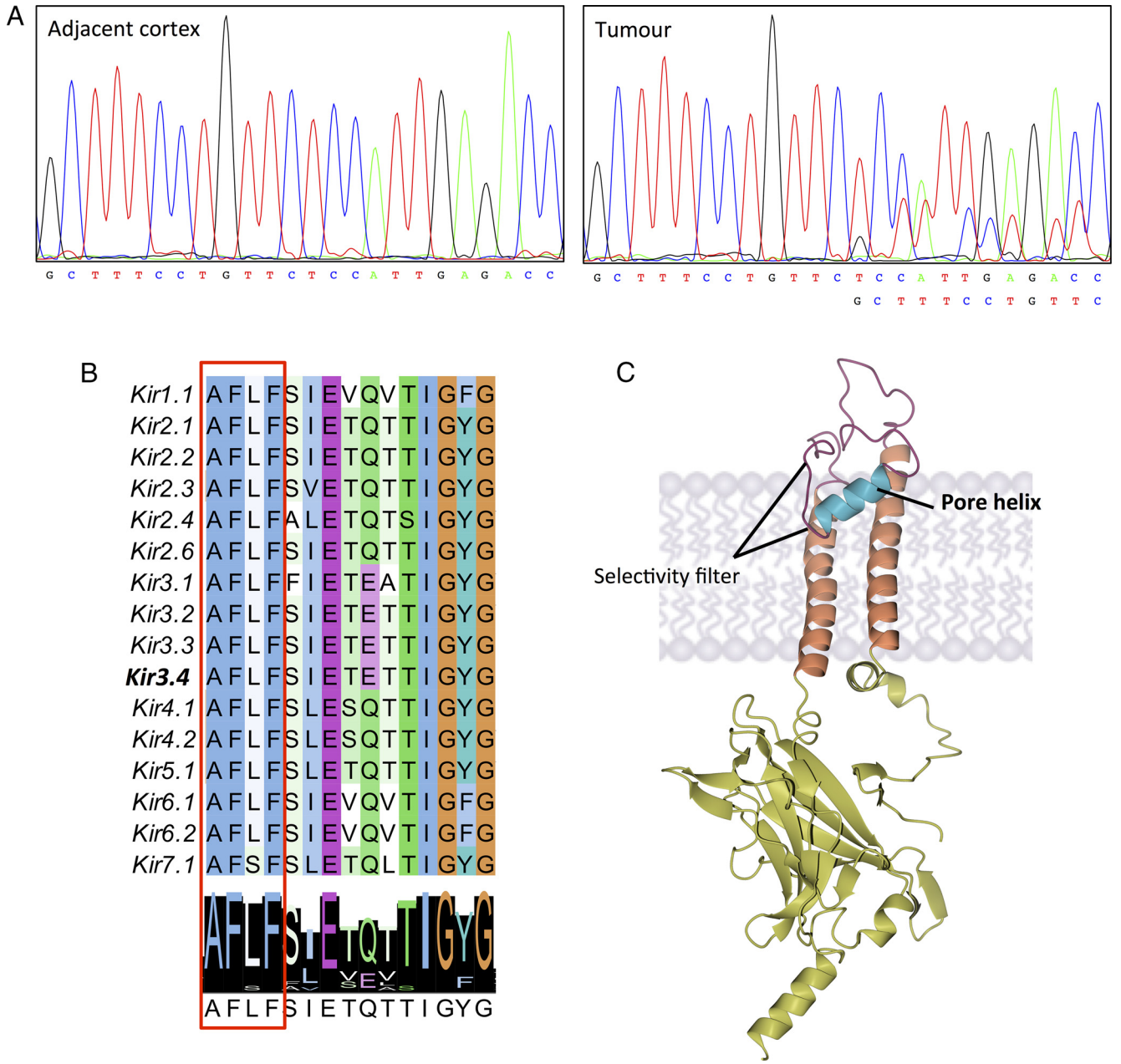

Figure 1. A novel somatic 12-bp duplication mutation in *KCNJ5* leads to the expansion of the highly conserved pore helix of GIRK4. A, Chromatograms of partial *KCNJ5* sequences from a patient's normal adjacent cortex and tumor genomic DNA. B, Protein sequence alignment and consensus sequence of Kir family members (using CLUSTAL omega), the duplicated region is highlighted by a red box. C, A homology model of GIRK4 embedded into the plasma membrane, highlighting the selectivity filter and downstream pore helix containing the mutation.

alized to the left side on adrenal venous sampling. The left adrenal was excised laparoscopically, and histological examination of the APA showed an adenoma in which zona fasciculata-like cells predominated with faint GIRK4 staining throughout the tumor section (Supplemental Figure 1).

Electrophysiological characterization of the novel A139_F142dup

To characterize the functional properties of the novel mutant A139_F142dup-GIRK4 channel, it was coexpressed with wild-type GIRK1 in *Xenopus* oocytes. The cholinergic muscarinic receptor 2 (M2R) was also coexpressed to provide evidence for the incorporation of GIRK4 subunits into functional channels and to study the impact of intracellular $G_{\beta\gamma}$ units from the $G_{i/o}$ family on channel activity. Both wild-type and A139_F142dup GIRK4 exhibited an inwardly rectifying K^+ current that had increased peak intensity in the presence of carbachol (CCh) and was inhibited by 3 mM Ba^{2+} (Figure 2A and Supplemental Figure 2). Neither the basal K^+ current nor the CCh-stimulated increase was seen in oocytes express-

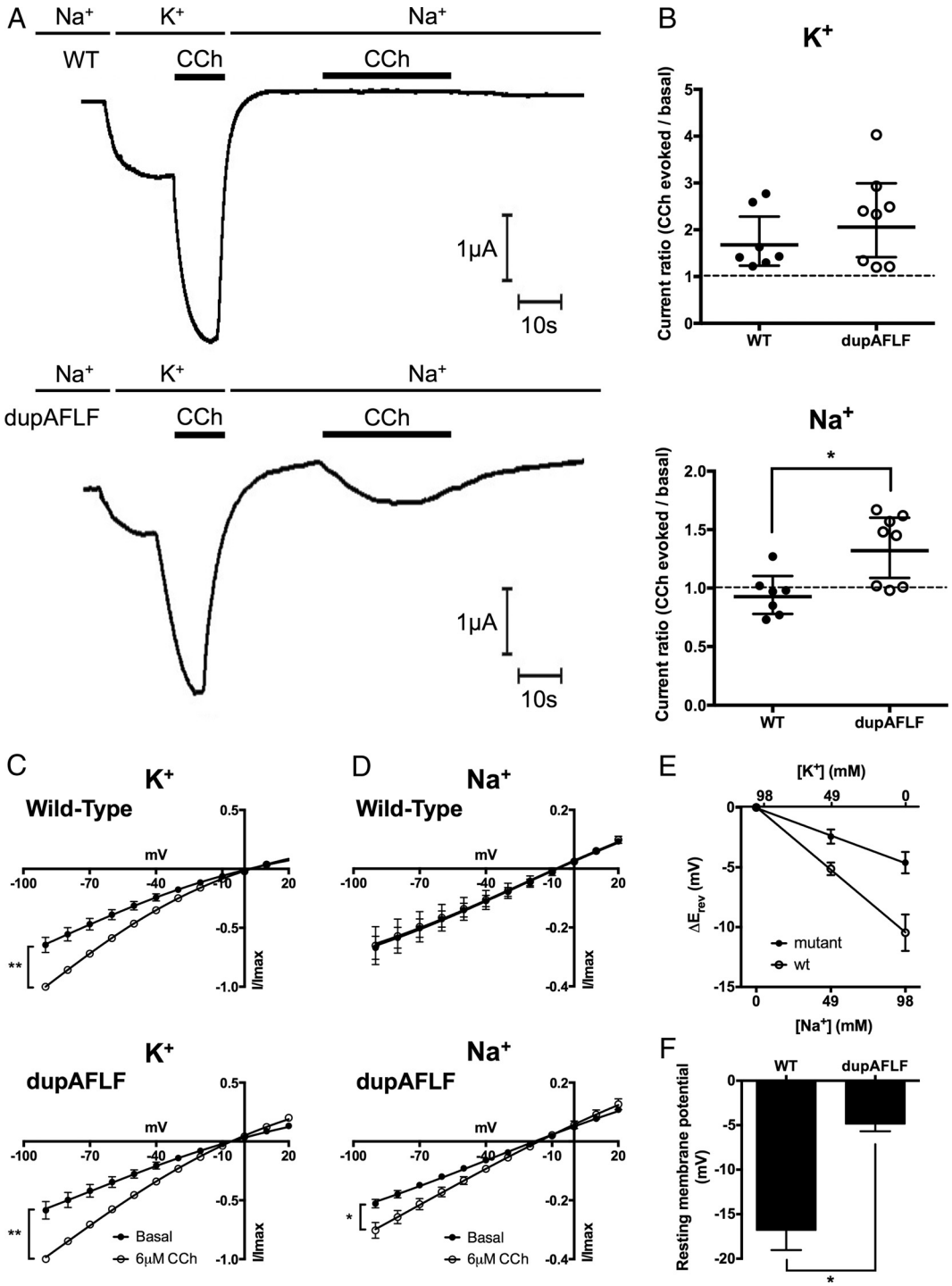

Figure 2. Functional characterization of dupAFLF-GIRK4 shows CCh induced Na^+ currents and reduced selectivity. A, Continuous current recordings of oocytes held at −80 mV, expressing either wild type (WT) or dupAFLF-GIRK4 coinjected with M2R and GIRK1. Oocytes were exposed to bath solutions containing either 98 mM Na^+ or 98 mM K^+ with 6 μM CCh. B, Ratios of CCh evoked vs basal current for at least seven oocytes expressing wild type or dupAFLF-GIRK4 with M2R and GIRK1 in 98 mM K^+ or 98 mM Na^+ bath solutions. Error bars represent mean ± 95% confidence interval. *, $P < .05$ by unpaired *t* test. C and D, I-V plots of the mean of seven oocytes expressing wild type or dupAFLF-GIRK4 with M2R and GIRK1. Oocytes were clamped at voltages from −90 mV to +20 mV in 10-mV steps. Voltage families were recorded in 98 mM K^+ (C) or 98 mM Na^+ (D) bath solutions with or without the addition of 6 μM CCh. Currents were normalized to the maximal current for each oocyte and expressed relative to the maximal peak current (I/Imax). Error bars represent SEM of seven oocytes. *, $P < .05$, **, $P < .01$ by paired *t* test. E, E_{rev} in oocytes expressing wild type or dupAFLF-GIRK4 along with M2R and GIRK1, in three solutions containing 98 mM K^+, 49 mM K^+ with 49 mM Na^+, and 98 mM Na^+. Error bars represent mean ± SEM of at least 26 oocytes. F, Resting membrane potential of oocytes expressing wild type or dupAFLF-GIRK4. Error bars represent mean ± SEM of at least five oocytes. *, $P < .005$ by unpaired *t* test.

ing GIRK1 and M2R alone (Supplemental Figure 3). In contrast to wild-type GIRK4-expressing oocytes, those expressing A139_F142dup-GIRK4 also exhibited a CCh-induced Na^+ current (Figure 2, A and B), indicating that A139_F142dup-GIRK4 channels had substantial Na^+ permeability. This was consistent with the changes in the I-V relationship of wild-type and mutant GIRK4 when switching between high external K^+ (K_e = 98 mM) and high external Na^+ (Na_e = 98 mM) solutions (Figure 2E). I-V plots of oocytes expressing wild type and A139_F142dup-GIRK4 exhibited similar inward rectification and reversal potential (E_{rev}) of both their basal K^+ and CCh-stimulated currents in high external K^+ (Figure 2C). In the high external Na^+ solution, both oocytes expressing wild type and dupAFLF-GIRK4 did not show inward rectification of basal or CCh-stimulated currents (Figure 2D). In contrast to wild-type GIRK4, mutant GIRK4 showed reduced negative shifts in E_{rev} when I-V relationships were measured in high external Na^+ and K^+ (Figure 2E). The resting membrane potentials of oocytes expressing dupAFLF-GIRK4 were also significantly increased compared with wild-type expressing oocytes (Figure 2F).

Expression and localization of A139_F142dup-GIRK4

Expression of GIRK4-GFP in mammalian HeLa cells showed that it localized to the plasma membrane, but there was a marked reduction in the expression of A139_F142dup-GIRK4-GFP compared with wild-type GIRK4-GFP (Figure 3A). Biotinylation of cell surface proteins in GIRK4-GFP-transfected HEK293T cells confirmed it was expressed at the plasma membrane (Figure 3B) and that total expression was decreased (Figure 3C). A higher-molecular-weight band was detected in the biotinylated sample for the wild-type channel, at a size predicted for the GIRK4 tetramer, despite the denaturing environment of the gel. This band was absent for the mutant channel, suggesting that tetramer stability was markedly reduced. Decreased expression was also observed by flow cytometry (Supplemental Figure 4), in which cells expressing mutant GIRK4 showed a marked increase in side scatter compared with wild-type cells. This suggests changes to intracellular morphology possibly as a result of increased degradation (Supplemental Figure 5).

Aldosterone release from H295R cells

To determine the effect of A139_F142dup-GIRK4 on adrenal cortical cell function. this mutant was expressed in H295R cells, which express endogenous GIRK1. These are currently the most relevant human cells to model the zona glomerulosa, and they produce aldosterone under basal conditions, with increased production following stimulation with angiotensin II (15). Strikingly, cells expressing A139_F142dup-GIRK4 had a significantly higher aldosterone production rate (2.3-fold, $P < .005$) than cells transfected with vector alone (negative control) or wild-type- and delI157 (a typical missense selectivity filter *KCNJ5* mutant used as positive control)-expressing cells (Figure 4), without any measurable effects on cell viability (Supplemental Figures 4). Of note, there was no further increase in aldosterone production from cells expressing A139_F142dup-GIRK4 when exposed to 10 nM angiotensin II, suggesting maximal aldosterone production was possible without involvement of the angiotensin II type 1 receptor pathway. This was distinct from the behavior of delI157-GIRK4, which is a typical missense selectivity filter mutant and associated with increased angiotensin II evoked release in the H295R (Figure 4).

Discussion

Through *KCNJ5* sequencing of our cohort of patients with APAs, we have confirmed the importance of somatic mutations in *KCNJ5* with almost half (45%) of the surgically recovered tumors in the cohort having a somatic mutation. We also identified a novel somatic mutation that caused a 12-bp duplication (A139_F142dup) affecting the pore helix and not the selectivity filter of GIRK4. Yet, in keeping with previous *KCNJ5* mutants within the selectivity filter, this duplication leads to abnormal Na^+ permeability and enhances aldosterone release from H295R cells. In contrast to previous mutants, this duplication displays a Na^+ current in the presence of a G-protein receptor agonist, and although basal aldosterone production is increased in cells harboring this mutation, it is not affected by angiotensin II. This suggests that endogenous levels of $G_{\beta\gamma}$ proteins in the H295R cells are sufficient to activate the mutant GIRK4. The lack of an aldosterone response to angiotensin II in the transfected H295R cells also mirrors closely the behavior of the APA in this patient: specifically there was no rise in aldosterone on standing, thereby classifying it as an angiotensin II-unresponsive APA (17). This lack of a postural aldosterone response is a feature we previously reported in APAs bearing *KCNJ5* somatic mutations (16) and is typical of APAs with zona fasciculata-predominant histology as we saw in our patient (17).

The AFLF motif that is duplicated in this novel somatic mutant is highly conserved in all members of the inwardly rectifying potassium channels apart from a single amino acid difference in the Kir7.1 channel (see alignment in

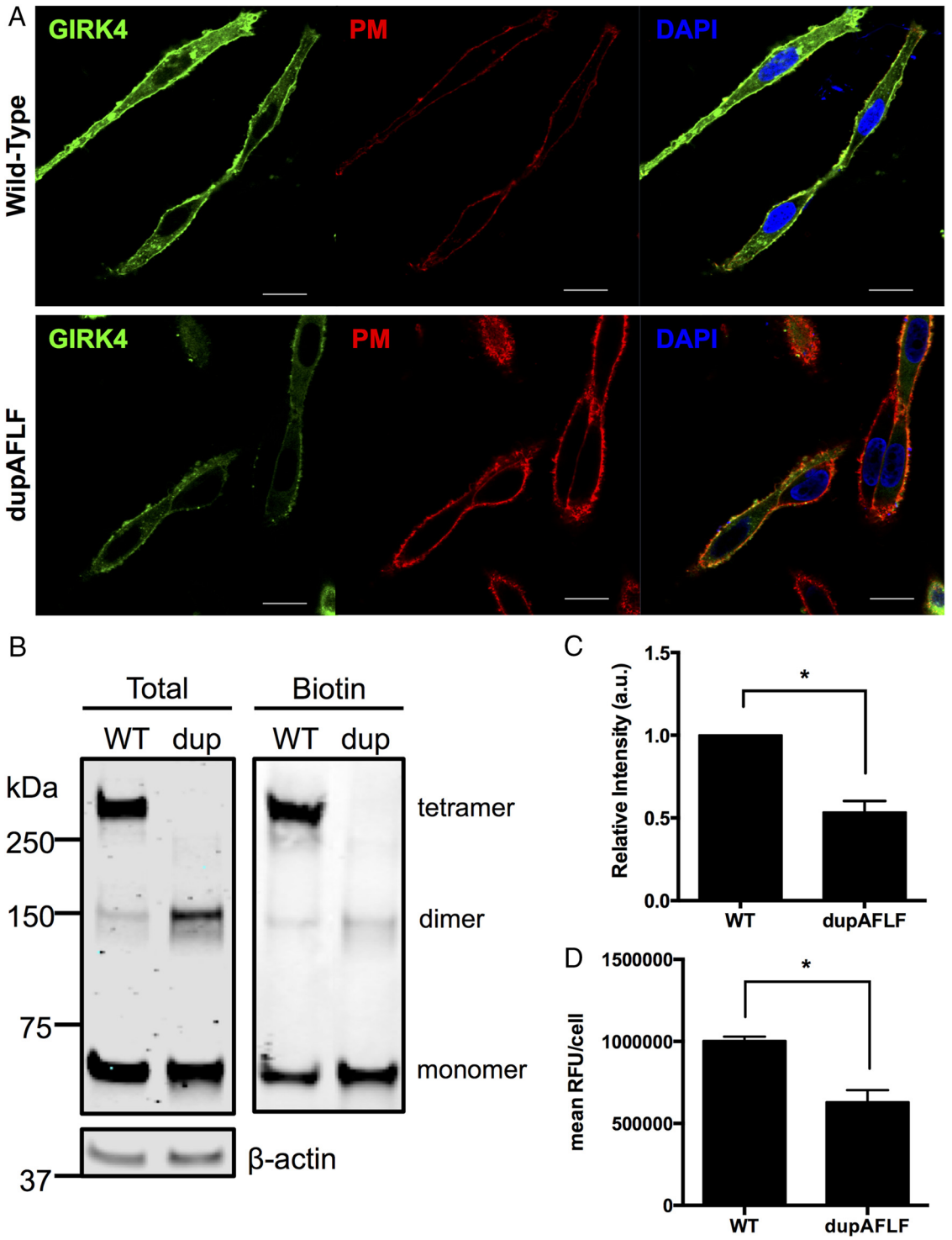

Figure 3. Reduced expression and stability of dupAFLF-GIRK4 in mammalian cell lines. A, Confocal microscopy of HeLa cells expressing wild type or dupAFLF-GIRK4-GFP. Plasma membrane (PM) stained with WGA 594, GIRK4 visualized by using a GFP-tag, and nuclei stained with 4′,6′-diamino-2-phenylindole (DAPI). B, Total and cell surface biotinylated proteins from HEK293T cells expressing GIRK4-GFP wild type or dupAFLF. Anti-GIRK4 antibody detected three bands with molecular weights that were consistent with tetramer, dimer, and monomer forms of GIRK4. As a loading control, β-actin was stained. C, Quantification of Western blot showing total GIRK4 expression in HEK293T cells expressing wild type or dupAFLF-GIRK4-GFP. Error bars represent mean ± SEM of three Western blots. *, $P < .05$ by unpaired *t* test. D, Relative fluorescent units of HEK293T cells expressing wild type or dupAFLF-GIRK4-GFP measured by flow cytometry. Error bars represent SEM of independent experiments, each with 10 000 events. *, $P < .05$ by unpaired *t* test.

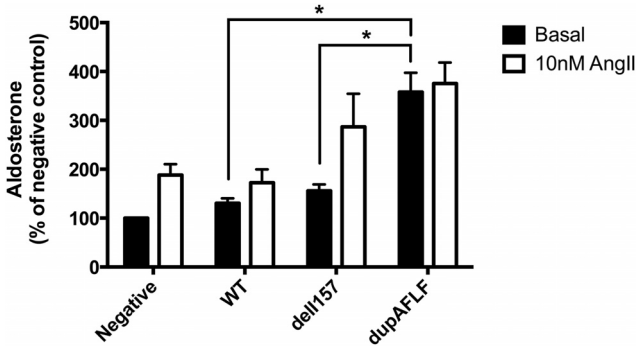

Figure 4. Angiotensin-independent increase in aldosterone secretion in cells expressing dupAFLF-GIRK4. Aldosterone secretion from H295R cells expressing GIRK4-GFP wild type, delI157 (positive control), and dupAFLF over 24 hours, with or without 10 nM angiotensin II stimulation. Error bars represent mean ± SEM of at least five independent experiments *, $P < .05$ calculated by a two-way ANOVA.

Supplemental Figure 5). The AFLF motif forms part of the pore helix, a short helix that extends away from the selectivity filter residues, and the structure of this helix (like the AFLF motif) is again highly conserved in evolutionary terms, being present in a range of non-Kir K^+ channels including the precursor bacterial KcsA (3) (see alignments in Supplemental Figure 6). The importance of the pore helix can be seen from mutation of the E147 residue at the base of the pore helix (between the AFLF motif and the selectivity filter). The E147Q mutant shows a striking loss of the bursting behavior that characterizes the open state of the GIRK4 ion channel (18). Intriguingly, the fast transitions between the open and closed state in these bursts are destabilized, but the E147Q channel importantly retains its K^+ selectivity. Hence, we suspect that the duplication of the AFLF motif alters the tertiary structure near the selectivity filter and disrupts its cation selectivity directly, rather than through loss of pore helix function per se.

The novel A139_F142dup mutant has increased Na^+ permeability that is most obvious in the presence of an agonist. There are, however, other aspects of its behavior that are distinct from somatic mutations that lie within the selectivity filter. Specifically, when expressed in mammalian cells, A139_F142dup-GIRK4 is effectively transported to the plasma membrane but has reduced expression at the cell surface. We saw significant basal currents in the oocytes expressing the dupAFLF mutant, suggesting robust surface expression. However, this is misleading because oocytes have lax processing and trafficking of channel proteins to the membrane and often poorly predict surface expression in the more rigorous mammalian cell system (19). Indeed, our confocal imaging in HeLa cells actually showed reduced expression of A139_F142dup-GIRK4 (Figure 2) that is confirmed by both biotinylation and blotting in another mammalian line (HEK cells, Figure 3) as well as flow cytometry in the same line expressing GFP-tagged wild type vs the dup AFLF mutant channel (Supplemental Figure 3). Other somatic mutations (R115W and E246G) have been reported to have reduced abundance at the cell surface that the authors speculated was due to reduced membrane insertion (20). However, our data suggest that reduced expression of our duplication mutant may be due to reduced stability of the mature GIRK channel in the membrane itself. Reduced expression was also observed in the adenoma tissue of the patient, suggesting that the 12-bp duplication in the pore helix leads to conformational changes in the protein structure, which affect stability and presumably lead to higher turnover rates. Although a recent study has identified reduced expression of GIRK4 staining in many APAs bearing somatic *KCNJ5* mutations (21). However, despite reduced stability, when expressed in H295R cells, the novel duplication mutation is capable of substantially increasing basal aldosterone secretion. This increase in aldosterone secretion is consistent with depolarization of cells expressing AFLF-GIRK4 and is confirmed in the oocyte studies in which the cells are markedly depolarized by the mutant channel.

A remaining puzzle for APAs is how a depolarizing channel mutation is able to drive clonal expansion and hence adenoma formation. It has been suggested that calcium influx is the key player (3), but changes in cell viability that this might cause have not been seen in all studies and we could not demonstrate altered cell viability of H295R cells expressing the dupAFLF mutant KCNJ5. A recent study has shown that clusters of adrenal cortical cells (APCCs) that overexpress the CYP11B2 aldosterone synthase are actually common in normal adrenal glands (22). These APCCs also appear to frequently harbor somatic driver mutations such as those reported here in KCNJ5. So the question now becomes, what second hits to the genome of these APCCs steers them toward clonal expansion? Further work is needed to understand the molecular events in play, but it must be a common pathophysiological event, given the high prevalence of APAs in the hypertensive population.

In summary then, we have confirmed that *KCNJ5* somatic mutations are very common mutations in APAs removed in our center, and this supports the contention by Williams et al (23) that they are the most common gene variation in APAs. We have also identified a novel mutation in the pore helix of the channel not previously reported as a site for somatic KCNJ5 mutations. This mutant has a distinct phenotype from those previously reported. In particular, it causes loss of K^+ selectivity and affects GIRK channel stability, but it is still able to constitutively increase aldosterone production by H295R

cells. This mutation extends our knowledge of how the KCNJ5 mutation can drive autonomous secretion from APAs in subjects with PA.

Acknowledgments

Address all correspondence to: K. M. O'Shaughnessy, MD, PhD, Division of Experimental Medicine and Immunotherapeutics, Level 6, ACCI Building, Addenbrookes Hospital, Cambridge CB2 2QQ, United Kingdom. E-mail: kmo22@medschl.cam.ac.uk.

This work was supported by the British Heart Foundation (PhD studentship to IH FS 12/78/29875), the Princess Alexandra Research Foundation, and the Irene Patricia Hunt Memorial Trust for Hypertension Research.

Disclosure Summary: The authors have nothing to disclose.

References

1. **Funder JW, Carey RM, Fardella C, et al.** Case detection, diagnosis, and treatment of patients with primary aldosteronism: an Endocrine Society Clinical Practice Guideline. *J Clin Endocrinol Metab*. 2008;93(9):3266–3281.
2. **Mulatero P, Stowasser M, Loh KC, et al.** Increased diagnosis of primary aldosteronism, including surgically correctable forms, in centers from five continents. *J Clin Endocrinol Metab*. 2004;89(3):1045–1050.
3. **Choi M, Scholl UI, Yue P, et al.** K+ channel mutations in adrenal aldosterone-producing adenomas and hereditary hypertension. *Science*. 2011;331(6018):768–772.
4. **Lenzini L, Rossi GP.** The molecular basis of primary aldosteronism: from chimeric gene to channelopathy. *Curr Opin Pharmacol*. 2015;21(0):35–42.
5. **Zheng F-F, Zhu L-M, Nie A-F, et al.** Clinical characteristics of somatic mutations in Chinese patients with aldosterone-producing adenoma. *Hypertension*. 2015;65(3):622–628.
6. **Taguchi R, Yamada M, Nakajima Y, et al.** Expression and mutations of KCNJ5 mRNA in Japanese patients with aldosterone-producing adenomas. *J Clin Endocrinol Metab*. 2012;97(4):1311–1319.
7. **Wang B, Li X, Zhang X, et al.** Prevalence and characterization of somatic mutations in chinese aldosterone-producing adenoma patients. *Medicine (Baltimore)*. 2015;94(16):e708.
8. **Geller DS, Zhang J, Wisgerhof MV, et al.** A novel form of human mendelian hypertension featuring nonglucocorticoid-remediable aldosteronism. *J Clin Endocrinol Metab*. 2008;93(8):3117–3123.
9. **Akerstrom T, Crona J, Delgado Verdugo A, et al.** Comprehensive re-sequencing of adrenal aldosterone producing lesions reveal three somatic mutations near the KCNJ5 potassium channel selectivity filter. *PloS One*. 2012;7(7):e41926.
10. **Wickman K, Nemec J, Gendler SJ, et al.** Abnormal heart rate regulation in GIRK4 knockout mice. *Neuron*. 1998;20(1):103–114.
11. **Kennedy ME, Nemec J, Corey S, et al.** GIRK4 confers appropriate processing and cell surface localization to G-protein-gated potassium channels. *J Biol Chem*. 1999;274(4):2571–2582.
12. **Monticone S, Hattangady NG, Nishimoto K, et al.** Effect of KCNJ5 mutations on gene expression in aldosterone-producing adenomas and adrenocortical cells. *J Clin Endocrinol Metab*. 2012;97(8):E1567–E1572.
13. **Murthy M, Azizan EA, Brown MJ, et al.** Characterization of a novel somatic KCNJ5 mutation delI157 in an aldosterone-producing adenoma. *J Hypertens*. 2012;30(9):1827–1833.
14. **Murthy M, Xu S, Massimo G, et al.** Role for germline mutations and a rare coding single nucleotide polymorphism within the KCNJ5 potassium channel in a large cohort of sporadic cases of primary aldosteronism. *Hypertension*. 2014;63(4):783–789.
15. **Brenner T, O'Shaughnessy KM.** Both TASK-3 and TREK-1 two-pore loop K channels are expressed in H295R cells and modulate their membrane potential and aldosterone secretion. *Am J Physiol Endocrinol Metab*. 2008;295(6):E1480–E1486.
16. **Azizan EA, Murthy M, Stowasser M, et al.** Somatic mutations affecting the selectivity filter of KCNJ5 are frequent in 2 large unselected collections of adrenal aldosteronomas. *Hypertension*. 2012;59(3):587–591.
17. **Ganguly A, Dowdy AJ, Luetscher JA, et al.** Anomalous postural response of plasma aldosterone concentration in patients with aldosterone-producing adrenal adenoma. *J Clin Endocrinol Metab*. 1973;36(2):401–404.
18. **Alagem N, Yesylevskyy S, Reuveny E.** The pore helix is involved in stabilizing the open state of inwardly rectifying K(+) channels. *Biophys J*. 2003;85(1):300–312.
19. **Moeller HB, Fenton RA.** Can one 'bad egg' really spoil the batch? *J Physiol*. 2010;588(13):2283–2284.
20. **Cheng C-J, Sung C-C, Wu S-T, et al.** Novel KCNJ5 mutations in sporadic aldosterone-producing adenoma reduce Kir3.4 membrane abundance. *J Clin Endocrinol Metab*. 2015;100(1):E155–E163.
21. **Fernandes-Rosa FL, Amar L, Tissier F, et al.** Functional histopathological markers of aldosterone producing adenoma and somatic KCNJ5 mutations. *Mol Cell Endocrinol*. 2015;408(0):220–226.
22. **Nishimoto K, Tomlins SA, Kuick R, et al.** Aldosterone-stimulating somatic gene mutations are common in normal adrenal glands. *Proc Natl Acad Sci USA*. 2015;112(33):E4591–E4599.
23. **Williams TA, Monticone S, Mulatero P.** KCNJ5 mutations are the most frequent genetic alteration in primary aldosteronism. *Hypertension*. 2015;65(3):507–509.